RSC Advances

PAPER

View Article Online
View Journal | View Issue

Cite this: *RSC Adv.*, 2023, **13**, 30680

Preparation of fluffy bimodal conjugated electrospun poly(lactic acid) air filters with low pressure drop

Minggang Lin,[ab] Jinlin Shen,[bc] Bingbing Wang,[bc] Yangyi Chen, *[bc] Chuyang Zhang[abc] and Huan Qi *[bc]

Electrospun nanofiber membranes have been extensively studied as air filters. However, their limited filtration efficiency for submicron inhalable particulate matter (PM), high resistance to filtration, and limited capacity to hold dust have hindered their widespread use. The majority of materials come from petroleum, and the use of organic solvents during the spinning process has a significant negative impact on the environment. In this work, a sustainable method has been proposed for producing filters using poly(lactic acid) (PLA) with a bimodal diameter distribution through conjugated electrospinning. This technique allows for the continuous production of interconnected micro/nano hybrid porous membranes, resulting in reduced resistance and improved dust holding capacity. The filtration efficiency, pressure drop, long-term filtration performance, and actual performance of the conjugated bimodal membrane (CBM) were extensively investigated. The results indicate that the filter has a high capacity for retaining particles, with filtration efficiencies of 99.94% for PM 0.3 and 99.96% for PM 2.5. It also demonstrates a high quality factor (0.078 Pa^{-1} for PM 0.3 and 0.084 Pa^{-1} for PM 2.5), long-term stability (a decrease of 2.35% for PM 0.3 and 0.05% for PM 2.5 over a period of 60 days) and outstanding dust holding capacity (9.17 g m^{-2}). The conjugated bimodal membrane (CBM) shows a 22.64% decrease in resistance compared to the non-conjugated bimodal membrane (BM). In general, the approach outlined in this work provides valuable insights into the development of high-performance biodegradable air filters. These filters have improved filtration efficiency and reduced resistance.

Received 1st September 2023
Accepted 11th October 2023

DOI: 10.1039/d3ra05969c

rsc.li/rsc-advances

1. Introduction

Long-term exposure to air pollution and particulate matter (PM) can cause individuals to develop pneumoconiosis and other diseases.[1,2] Small airborne particles, such as PM 2.5 and PM 0.3 (with a diameter of less than 2.5 μm and 0.3 μm), can bypass the body's defenses and enter our respiratory and circulatory systems. This can result in damage to our lungs, heart, and brain, making it crucial to address air pollution to safeguard public health.[3] The rapid development of industrialization has brought about some drawbacks, such as dust storms, which have made people more aware of the need for personal protection. The mask interface material, which is a critical component of respiratory equipment and a vital barrier, captures and filters solid and liquid aerosols. According to the Global Times News, during the COVID-19 pandemic, approximately 129 billion people worldwide use masks every month, with a usage rate of 3 million masks per minute.[4,5] As a result, there is an increased demand for efficient and environmentally friendly filtration materials in daily life. There has been a tendency in research into the development of high-performance filter.[6–8]

Meltblown nonwovens and electrospun nonwovens are just two of the many filtration materials that make up a significant part of the global market. The production of meltblown nonwoven is more complex and requires polymers with low viscosity and high flow index.[9] In addition, meltblown fabrics typically have fiber diameters in the range of 1–5 μm.[10,11] The use of corona discharge electret technology is necessary to impart electrostatic capability to the interlayer of typical commercial masks in order to achieve satisfactory filtration performance. However, the electret charge is prone to escaping.[12] The combination of microfibers and nanofibers is an effective method for achieving high efficiency and low resistance. This is because the prepared fiber membranes have small pore sizes, high porosity, and universality. However, the process of preparing stacked micro-nanofiltration membranes requires layer-by-layer assembly, which makes the preparation process complex.[13,14]

Many of the materials used for daily protection are made from petroleum-based products, posing a significant threat to

[a]College of Textile and Apparel, Xinjiang University, Urumqi 830000, Xinjiang, China
[b]Institute of Smart & Ecological Textile, Quanzhou Normal University, Fujian 362002, China
[c]College of Textiles and Apparel, Quanzhou Normal University, Fujian 362002, China. E-mail: qhqh123@126.com; chenyangyi2008@163.com

the environment. These have a short life cycle and are frequently replaced.[15] In addition, these raw materials are not readily biodegradable and take a long time to decompose. It is therefore essential to use polymers that can replicate the properties of existing plastics. Polylactic acid (PLA) is derived from sustainable resources such as straw and plant starch. PLA has remarkable biodegradability, biocompatibility and mechanical properties comparable to those of traditional petroleum-based polymers.[16] This aspect makes it one of the most promising biodegradable polymers currently known, serving as an effective alternative. The use of disposable protective products has a clear advantage that is in line with the global trend towards environmentally friendly practices. It is therefore a form of environmentally friendly material with great potential for development.[17] However, research on PLA melt-blown nonwovens is still ongoing and its main drawback is low strength and insufficient tactile properties. As a result, electrospinning is still the main method used for PLA filter membrane materials.[18–20]

Electrospinning nanofibers are widely used in air filtration,[21] oil-water separation,[22] and water purification.[23,24] The technique involves applying a high-voltage electric field to a jet of solution in order to draw it into nanofibers.[25,26] The utilization of conjugate electrospinning, combined with the application of positive and negative voltages, results in the deposition of nanofibers onto the roller after the neutralization of the electrical charges. With an increase in membrane thickness, the surface charges decrease, leading to the formation of a three-dimensional nanofiber scaffold through continuous fiber deposition.[27] Furthermore, the electrospun nanofibers within the two syringes form a voluminous fiber bundle or even a large 3D nanofiber sphere in the central plane during polymer jetting and continuous injection driven by airflow. Tang *et al.* fabricate electrospun PLA fibers with conjugated, specific protrusions in one step to construct bimodal fibers.[28] Wang *et al.* fabricated double-layer hierarchical structured membranes with different mass ratios for further enhanced air filtration performance.[29] At present, conjugate electrospinning technology is mainly used for the production of nano-yarns and highly oriented membrane materials. It is less used for air filtration materials.[30]

Hence, we describe a straightforward and user-friendly method for producing PLA filter materials with a bimodal diameter distribution. This method effectively reduces filtration resistance and provides excellent air filtration capacity, as well as biodegradability and durability. Our design is characterized by the use of conjugated electrostatic spinning to continuously produce interconnected micro/nano fluffy membrane materials for filtration purposes. This fluffy structure enhances the physical interception of particulate matter by increasing the pore length. The fibers are distributed in a bimodal diameter distribution, which not only enhances the membrane's cavity structure but also effectively prevents the air channels from shrinking due to the small size of the fibers. This study systematically investigated the effects of membrane filtration performance, including filtration efficiency, pressure drop, long-term performance, and actual performance. We have utilized a solvent mixture that is relatively environmentally friendly to ensure the implementation of green chemistry throughout the entire process. Furthermore, we believe that this work holds great potential to serve as a valuable reference for the next generation of efficient, sustainable and environmentally friendly air pollution control.

2 . Materials and methods

2.1. Materials

Polylactic acid (REVODE110) was purchased from Zhejiang Haizheng Co., Ltd., (Taizhou, China). Ethyl acetate (EA) was purchased from Xilong Scientific Co., Ltd., (Shantou, China). *N*,*N*-Dimethylformamide (DMF) was supplied by Yien Chemical Technology Co., Ltd., (Shanghai, China). All chemicals were analytically pure and used without further purification.

2.2. Preparation of PLA membranes of bimodal fibers

The 12 wt% PLA solution was prepared by dissolving PLA pellets in a mixed solvent of ethyl acetate (EA) and dimethylformamide (DMF) in a ratio of 7 : 3 (v/v). The mixture was stirred continuously for 24 hours at 75 °C. The same volume of solution (4.0 mL) was consistently used for electrospinning using an electrospinning apparatus (SS-X3, Beijing Yongkang Co., Ltd., China). The solution flow rate was 1.0 and 3.0 mL h^{-1} through a flat-tipped 21-gauge needle (named M-1 and M-3). Double-needle parallel electrospinning involves placing two identical needles side by side for the spinning process. The needles are connected to the same voltage, but they have different spinning rates: 3.0 mL h^{-1} and 1.0 mL h^{-1} respectively. These rates are used to fabricate a membrane material with a bimodal distribution (named BM). Conjugate electrospinning is performed using two symmetrical needles controlled by positive and negative voltages. The symmetrically sprayed fibres are stretched by an electric field and then entangled to form fluffy 3D conjugate bimodal membranes (CBM) by passing through a lower-height receiving drum. The distance between the needle tip and the collector drum is maintained at 15.0 cm. The applied electric field can vary from 10.0 kV to 15.0 kV. The charged solution was then accelerated at a speed of 300 rpm (rotations per minute) onto the metal collector, which was wrapped with PLA spunbond nonwovens prepared in the laboratory.[17] The experiments were conducted at a temperature of 25.0 ± 3.0 °C and a relative humidity of 50.0 ± 10.0%. The membranes were then dried at 50 °C for 24 hours to eliminate remaining solvent.

2.3. Characterization

The surface morphology of the bimodal filter was investigated using a scanning electron microscope (TESAN MIRA LMS, Tescan China Ltd., China) after being coated with gold. The diameter and distribution of the PLA nanofibers were analyzed using Nano Measure 1.2. The thickness test was conducted using an AMES 99-0697 thickness tester. Ten replicates were performed for each sample and the mean values were recorded. The pore size distribution of the filter was measured using a capillary flow porometer (CFP-1500-AEXL, Porous Materials

Inc., Ithaca NY, USA). Air permeabilities of the filter samples were evaluated on an air permeability tester (YG461E, Quanzhou Meibang Instrument Co., Ltd.), in accordance with the ASTM D 737 standard. Five replications of each sample were tested, and the averages were reported. The porosity was calculated using eqn (1) based on the basis weight and thickness.

$$P = \left(1 - \frac{\text{Basis Weight}}{\text{Thickness} \times \rho_{\text{fiber}}}\right) \times 100\% \quad (1)$$

where P represent the porosity, and the density of polymer (PLA 1.24 g cm^{-3}), respectively.

Meanwhile, in order to evaluate the performance of the filter in effectively capturing particulate matter (PM), an independent filter tester was designed and constructed to simulate real-life haze conditions. The PM concentration was measured using a dust particle counter (AIRHUG-CP-15, Beijing Yishan Technology Co., Ltd.) to determine the actual filtration of PM concentrations on both sides of a burning cigarette.

2.4. Filtration performance measurement

The filtration efficiency and pressure drop were measured using an automated filter tester (DR251XL, Wenzhou Darong Textile Instrument Co., Ltd., Wenzhou, China). Charge-neutralized sodium chloride (NaCl) aerosol particles were generated from a 2.0 wt% NaCl aqueous solution. The particle sizes were normally distributed. The count median diameter of sodium chloride aerosol particles was 75 nm, and the geometric standard deviation of the particles was less than 1.86. They were dried after emerging from the Collision Nebulizer and then placed into the filter holder. Aerosol particles passed through the testing area of 100 cm^2 at a flow rate of 85.0 L min^{-1}. The concentration of NaCl aerosols was monitored by a photometer both upstream and downstream of the filters. The filtration efficiency (η) was calculated using the following eqn (2):

$$\eta = \frac{C_{\text{up}} - C_{\text{down}}}{C_{\text{up}}} \times 100\% \quad (2)$$

where C_{up} and C_{down} represent the concentration of NaCl aerosols in the upstream and downstream, respectively.

The quality factor (QF) is considered as a comprehensive parameter of filtration efficiency and pressure drop. The pressure drop of NaCl aerosols passing through the filter was continuously measured by the electronic pressure transmitter. QF can be calculated as the following eqn (3):

$$\text{QF} = -\frac{\text{Ln}(1-\eta)}{\Delta P} \quad (3)$$

where ΔP represents the pressure drop. Five different flat areas were selected for the test. The average values were used as the final data to evaluate the filtration performance.

The filtration loading test was performed to investigate the dynamic filtration properties according to GB 2626-2019. The concentration of NaCl aerosol was adjusted to a maximum of 20.0 mg m^{-3} and the air flow rate was adjusted to a maximum of 85.0 L min^{-1}. This determines the mass of particles deposited on the filter per unit area when the initial pressure drop doubles. The dust holding capacity has a significant influence on the service life of the air filter as it directly affects the frequency of filter replacements. It can be measured through a filtration loading test. The increase in weight of an air filter when the pressure drop reaches a specific value during a loading test reflects its dust-holding capacity. In addition, the storage stability was evaluated by testing the filtration efficiency after 60 days.

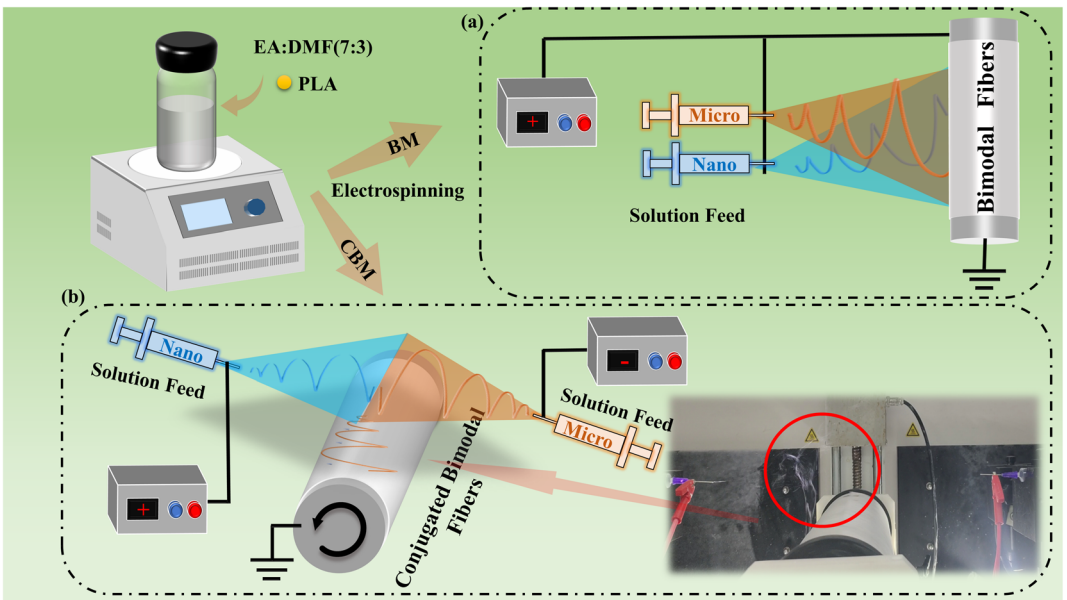

Fig. 1 Schematic illustration of the bimodal PLA membranes. (a) The double-spinneret parallel electrospinning process, and (b) the conjugated bimodal electrospinning membrane that with 3d structures.

3. Results and discussions

3.1. Structure design of bimodal PLA fibers

Currently, meltblown and electrospun materials are the most commonly used filters. The small size of the fibers ensures high capture efficiency for particles. However, the uniform fiber size in the filtration process can easily cause particles to accumulate and adhere to the surface layer of the filters. As a result, the filtration efficiency gradually increases while the resistance also rises significantly. Therefore, prolonging the passage of particles through the filter media and reducing the accumulation of particles in the surface layer can enhance the dust holding capacity of the filter media and decrease its filtration resistance. In order to achieve low breathing resistance, excellent high porosity properties, robust PM capture capacity, and long-term stability of air filters. The bimodal membranes are shown in Fig. 1. The design and manufacture of this high-performance biodegradable air filter were based on the following factors: (1) the membranes were made of biodegradable PLA using environmentally friendly organic solvents, which has significant environmental implications; (2) the utilization of two different fiber diameters for random blending, resulting in a filter with a bimodal distribution that combines the advantages of nanofiber and micron fiber blending, thereby enhancing filtration performance and reducing resistance; and (3) the implementation of a two-electrode stage model for the preparation of conjugated electrospinning membranes.[20] Two spinnerets are connected to positive and negative high-voltage power. The fibers spun from each side of the spinneret interact with each other, intertwining and connecting to form a three-dimensional network structure of fibers. This network structure directly affects the air permeability and pressure drop.

3.2. Morphology and structure analysis

SEM was used to analyze the morphology and fiber diameter of the filter. The morphology of the fiber membrane was shown in Fig. 2a and b. From the results, it was observed that the PLA fibers were interlaced with each other and the surface of the fibers appeared smooth and uniform with no beads deposited. The fiber diameters obtained at 1.0 and 3.0 mL h^{-1} were

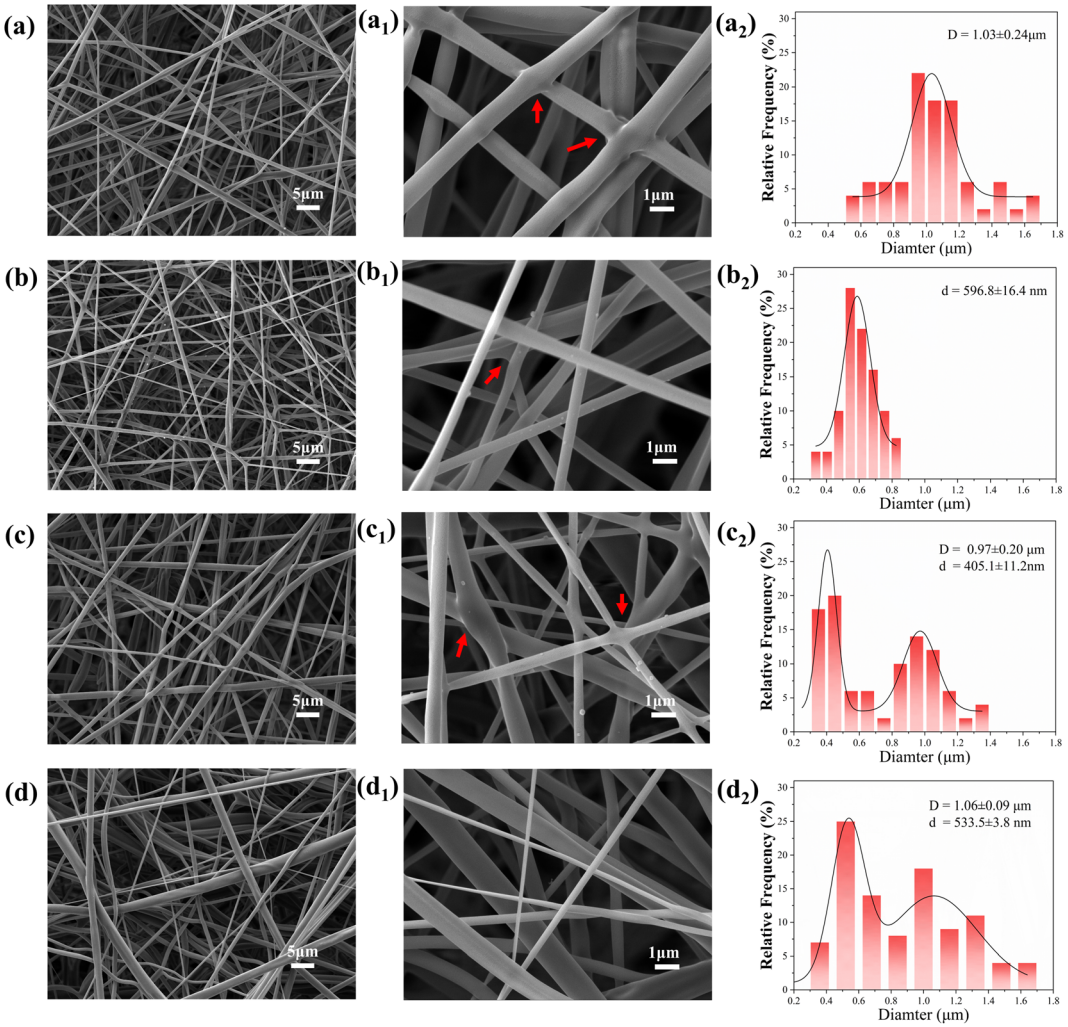

Fig. 2 SEM images and fiber diameter distribution diagrams of (a) M-1, (b) M-3, (c) BM and (d) CBM.

596.8 ± 16.4 nm and 1.03 ± 0.24 μm, respectively. Additionally, the fiber morphology was similar for M-1 and M-3, and the fiber diameters increased as the propulsion rate increased, which is consistent with the findings of their study.[31] Fig. 2c and d shows the fiber morphology and diameter of BM and CBM, indicating that the fiber membranes are composed of a homogeneous blend of micrometres (~1.0 μm) and nanofibers (~500.0 nm), both with a bimodal distribution as derived from the diameter distribution curves.[32,33] Interestingly, the CBM fibers exhibit a certain degree of fluffiness, lower fiber stacking density, and do not bond together like the M-1, M-3, and BM fibers. The use of ethyl acetate affects the degree of volatilization in the spinning process, which leads to the formation of a specific 3D structure of the CBM. Conjugate electrospinning can produce fibers with a fluffy fiber membrane structure. The bimodal distribution of fiber diameter obtained is very similar to that of M-1 and M-3, as both BM and CBM use the same spinning speed. The SEM illustrates the use of dual needles paired with different advancement speeds to form uniformly co-mingled bimodal micro/nanofibers.

3.3. Pore size and porosity

The interlacing of the fibres in the nonwovens creates pores which are critical to air filtering performance. The membrane's geometry, including porosity and pore size, plays a crucial role.

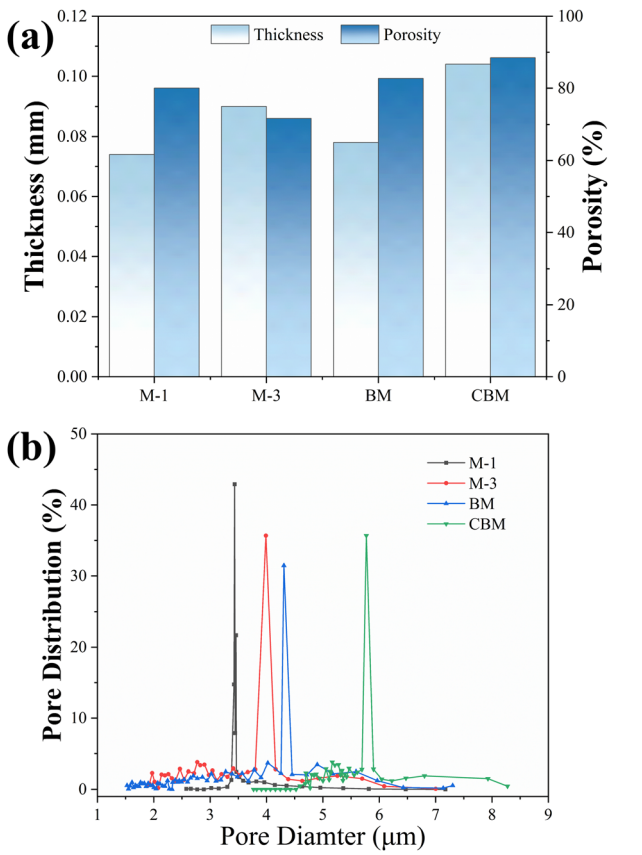

Fig. 3 (a) Porosity and thickness, and (b) the distribution of pore size of M-1, M-2, BM, and CBM.

As shown in Fig. 3a, larger fiber diameters result in membranes with smaller porosities. This is due to the smaller density of membrane solids per unit volume with larger diameters.[10] The CBM has a higher porosity (87.46%) compared to the BM (82.71%). This is due to the difference in structure between conjugated and non-conjugated membranes. As shown in Fig. 3b, conjugated membranes have a greater thickness at the same spinning volume. The pore size distributions for all four samples were found to be in the range of 2.0–8.0 μm, with the majority of pores concentrated in the 3.0–6.0 μm range. As fiber diameter increased, the main peak curve shifted to the right, and the average pore size decreased from 5.99 μm to 3.43 μm. The bimodal diameter distribution of fibers also exhibited an increasing trend in the main body pore size of the membranes. This could be due to the fact that fibers with different diameter distributions create more interfaces between layers. Additionally, the spacing between interfaces tends to be larger than the distance between inner fibers, which promotes the formation of more macropores. The main pore sizes for the BM and the CBM were 4.30 μm and 5.77 μm, respectively, as confirmed by conjugate electrospinning. Mixing fibers of different sizes was effective in avoiding excessive stacking density, which contributes to the formation of larger macropores. Moreover, the enlargement of the primary pores results in an increase in the average pore size. Overall, the bimodal membrane features an inter-fiber aperture that spans multiple scales. The development of bimodal fibers supports the creation of a comprehensive filtration medium and enhances filtration effectiveness. The increase in average pore size allows for easier airflow and reduces filtration resistance.

3.4. Filtration properties

The nanofiber membranes produced through electrostatic spinning for filtration materials typically exhibit superior filtration efficiency due to the production of nanoscale fibers. However, they also result in high air resistance and low dust holding capacity. Currently, reducing filtration resistance is focus research for nanofibers used in air filtration.[34,35] In this study, the membranes were able to significantly reduce air resistance while maintaining the same level of filtration efficiency. The efficiency was calculated by measuring the particle concentration of the sodium chloride aerogel upstream of the generator and downstream of the receiver sensor in Fig. 4a. The filtration efficiency of the membrane was extensively investigated at a flow rate of 85.0 L min^{-1} for PM 0.3. Filtration efficiency, pressure drop, and quality factor (QF) were used as evaluation parameters. Fig. 4b and c show the effect of varying fiber diameters. The filtration efficiencies of M-1, M-3, BM and CBM were 99.44%, 99.07%, 99.56%, and 99.94%, respectively. The corresponding resistances were 163.17 Pa, 138.00 Pa, 118.00 Pa, and 96.00 Pa. The membrane, which had a bimodal fiber diameter distribution, was observed to have a resistance of up to 118.00 Pa. However, by employing conjugated bimodal spinning, the resistance was decreased to 96.00 Pa. The fluffy conjugated bimodal electrostatic spinning technique can achieve a 41.20% reduction in filtration resistance. The QF is

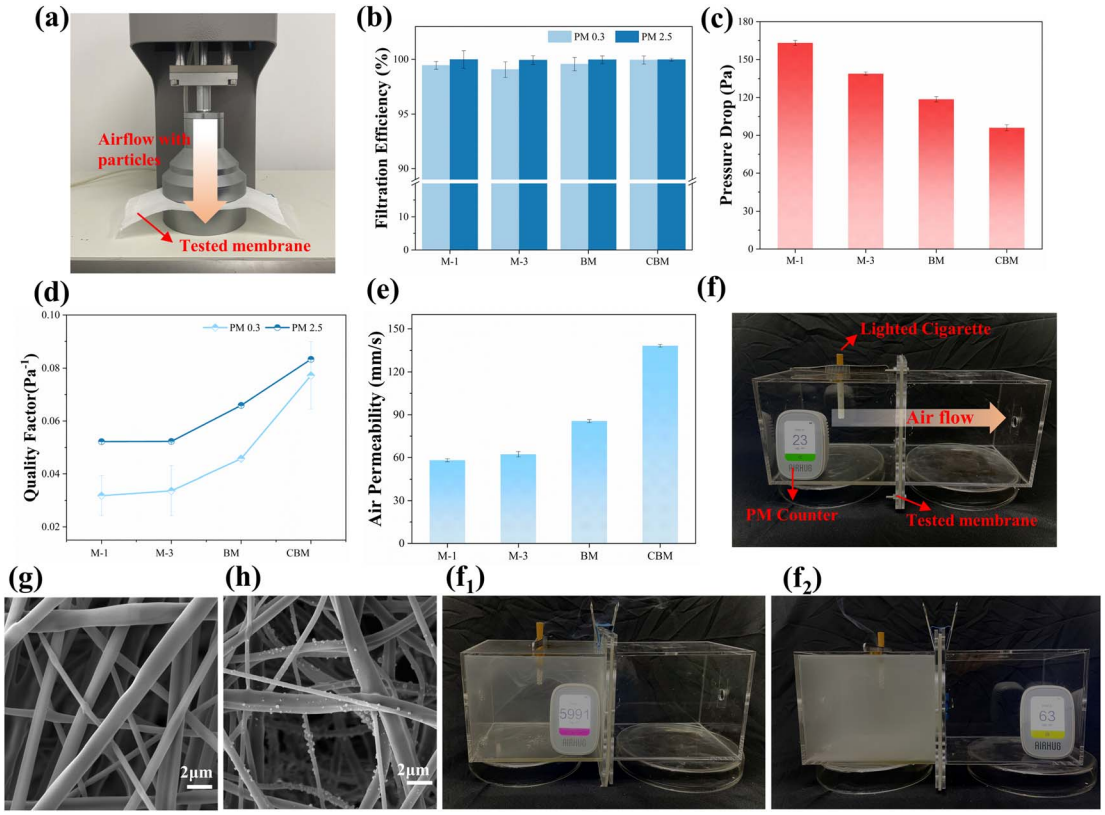

Fig. 4 (a) Diagram of air filtration equipment used to test the filtration efficiency, (b) filtration efficiency, (c) pressure drop, (d) quality factor, and (e) air permeability of M-1, M-2, BM, and CBM. (f) Filtration test system with the burning cigarette and a commercial particular counter, (f1 and f2) filtration test system with the burning cigarette the number of PM by the CBM, (g and h) SEM images of CBM before and after air filtration tests.

a measure of filtration efficiency and pressure drop, indicating the overall performance of filtration.[36] Fig. 4d shows that a fluffy and inhomogeneous structure results in a high QF with PM 0.3, reaching up to 0.078 Pa^{-1}. This is due to the efficient interception of nanofibers, which enhances the filtration process. As shown in Fig. 4e, the air permeability tests the effectiveness of the design of the conjugated bimodal membrane in enhancing gas flow, thereby reducing resistance. In Fig. 4g and h, the SEM images show the morphology of the fibers before and after filtration. NaCl aerogel is primarily captured and intercepted by the fine fibers. The microfiber enhances the slip effect, resulting in a smoother airflow. This effect is further improved by utilizing conjugated electrostatic spinning to create a three-dimensional structure with a fluffy texture. As a result, the airflow becomes even smoother. When the PM passes through, the diameter of the fiber and its fluffiness work together to affect the pressure drop, resulting in a significant reduction. The balance between filtration efficiency and pressure drop is critical when studying filtration materials. This differs from previous studies that were assembled by lamination.[37] The present method interweaves bimodal fibers in a blended form. This significantly reduces filter resistance while maintaining the same level of efficiency.

Smoke removal efficiency is also an important factor to consider for filter materials, particularly their ability to purify haze particles larger than PM 2.5. Therefore, we conducted simulations to determine the effectiveness of CBM in purifying smoke, as shown in Fig. 4f. A cigarette was lit on one side of the membrane and the CBM was placed in the middle of two transparent boxes with continuous ventilation. The concentration of smoke can be observed on both sides of the membrane during the combustion process. The PM produced on the left side filled the box, and the PM 2.5 counters on both sides of the membrane were tested separately. It can be seen that the CBM effectively intercepted and absorbed the PM in Fig. 4f1 and 2, which resulted in the right side of the box becoming clear and transparent. The left box has 5991.0 μg m^{-3} of PM 2.5, which is hundreds of times more than the right. The prepared membrane exhibits excellent filtration performance.

3.5. Loading performance and durability

To assess the stability and durability of PLA membranes for filtration purposes, tests were conducted to evaluate their performance in filtering PM 0.3 at different flow rates. These tests were conducted after the membrane had been in place for 60 days, along with load testing. Fig. 5a illustrates the impact of various airflow rates on the filtration performance. For the removal of particles PM 0.3, the filtration efficiency gradually decreased as the airflow rate increased from 25.0 L min^{-1} to 85.0 L min^{-1}. The CBM decreased from 99.91% to 97.85%, but it still remained above 95.00%. Fig. 5b shows that the pressure drop increased from 30.70 Pa to 96.10 Pa, indicating

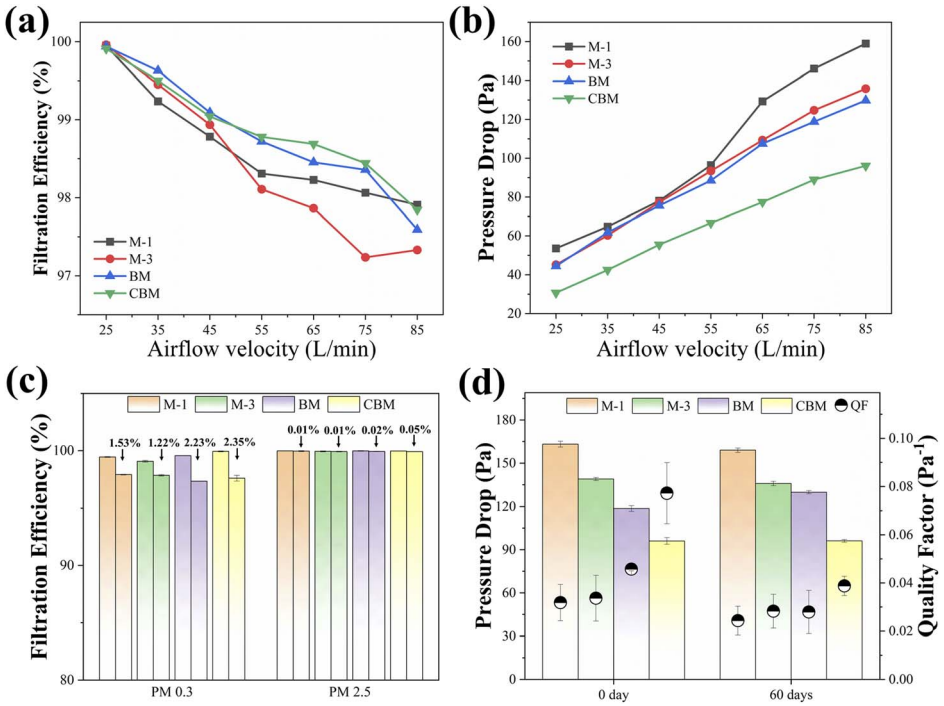

Fig. 5 (a) Filtration efficiency under various air flow rates, (b) pressure drop under various air flow rates of M-1, M-2, BM, and CBM. (c) Filtration efficiency after storage on 60 days with PM 0.3 and PM 2.5, (d) pressure drop and quality factor after storage on 60 days with PM 0.3.

a correlation with the increase in airflow velocity. This observation aligns with Darcy's law.[38,39] The positive relationship between pressure drop and airflow velocity suggests that the membrane material has open hair channels and exhibits excellent air permeability.

Fig. 5c reveals the changes in filtration efficiency and pressure resistance after 60 days in the room. The graphs depict the variations in PM 0.3 and PM 2.5 removal efficiencies. It can be inferred that the PM 2.5 filtration performance remains consistent even after 60 days, demonstrating a consistently high level of filtration efficiency. However, the PM 0.3 filtration performance decreased to different degrees, and the PM 0.3 filtration efficiency of CBM decreased from 99.94% to 97.59%, similar to the other membranes. This decrease may be attributed to the partial dissipation of surface charge, which occurs as a result of prolonged usage and a decrease in electrostatic adsorption. This finding was similar to a previous study.[40] After 60 days of storage, the filtration efficiency for PM0.3 changed from 99.94% to 97.59%, and the QF value changed from 0.078 Pa^{-1} to 0.039 Pa^{-1}. For PM 2.5, the filtration efficiency changed from 99.97% to 99.91%, and the QF value changed from 0.083 Pa^{-1} to 0.073 Pa^{-1} in Fig. 5d. The filter media still exhibits excellent and reliable filtration performance even after extended periods of storage. The filter media still maintains excellent and reliable filtration performance after long-term storage. The decrease in filtration efficiency demonstrates the superior storage stability of the micro- and nano-filter media. However, the CBM still maintains a very high filtration efficiency of 97.59%. This is because the electrostatic adsorption effect of the filter media is negligible compared to the mechanical interception effects, such as interception, inertial collision, Brownian motion, and gravitational deposition, which is supported by the fact that the filtration resistance remains essentially at a comparable level. Overall, due to the large size and weight of the particulate matter, interception and gravitational effects play a more prominent role in capturing it. The CBM provides optimum filtration for PM 2.5.

In actual use, the filter material may need to undergo continuous filtration for an extended period of time. Therefore, the stability of the dynamic filtration performance is crucial for the filter media.[41] We conducted a loading test on M-1 and CBM at a flow rate of 85.0 L min^{-1}, and the results are shown in Fig. 6a–c. In the loading test, the gas stream carrying sodium chloride aerosol (at a concentration of 20.0 mg m^{-3}) continuously rubbed against the filter media, resulting in deposition. As the amount of deposited particulate matter increased, the filtration resistance gradually increased. This increase in resistance was primarily due to depth filtration. The mechanical interception is enhanced because the trapped particles serve as deposition sites for subsequent particulate matter. Most importantly, the QF of the CBM was significantly higher than that of the M-1 during the entire load test period. Due to our unique design, the CBM offers better overall filtration performance than conventional electrospinning materials. Dust holding capacity is also an important indicator of filtration performance because it directly affects the frequency at which the filter material needs to be replaced. The high dust holding capacity reflects the filter media's retention capacity and its long service life. The Fig. 6d shows that M-1, M-1, BM, and CBM have values of 7.95 g m^{-2}, 5.02 g m^{-2}, 6.39 g m^{-2}, and 9.17 g m^{-2},

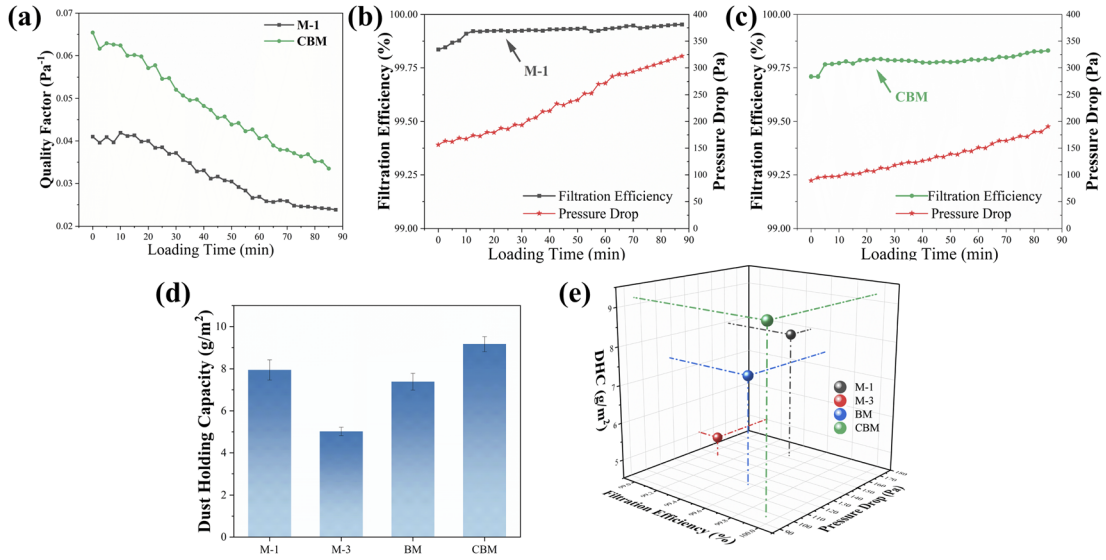

Fig. 6 (a) Quality factor during the loading test of M-1 and CBM, filtration efficiency and pressure drop during the loading test of (b) M-1 and (c) CBM. (d) Dust holding capacity against NaCl aerosol particles, (e) comparison of comprehensive filtration performance of M-1, M-3, BM and CBM.

respectively. It can be seen that CBM has a high dust-holding capacity. The CBM has better overall performance, excellent filtration performance, and a high dust holding capacity which gives it a long service life.

3.6. Filtration mechanism

Conjugated electrostatic spinning for the preparation of fibres with 3D structure conducive to excellent filtration performance. Under a positive and a negative high-voltage electric field, respectively, solutions initially expelled positively and negatively charged nanofibers. Nanofibers that were both charged were drawn to one another by the electric field. Using a conductive metal roll, which attracted entangled bimodal fibers and started fiber deposition onto the membranes. Specifically, bimodal fibers generated by high voltage were immediately deposited onto the metal collector roll. Subsequent fibers were then loosely accumulated on the previously deposited membranes, resulting in a stack of fibers. Initially, a thin membrane formed quickly on the collector due to the strong pulling force exerted by the grounded metal roll. The stack reached a certain height. At this stage, the dominant force driving fiber deposition was the presence of previously accumulated fibers on the surface of the collector. The surface charge gradually decreased with an increasing number of deposited fibers. This resulted in a weaker attraction to the as-spun nanofibers, causing relatively loose nanofibers on the surface compared to the initially deposited nanofibers in the inner part of the membranes.

The bimodal distribution of fluffy fibers creates a three-dimensional interpenetrating network structure, as shown in Fig. 7. This structure facilitates airflow and provides longer channels and more space, preventing the trapping of small particles. As a result, it can hold more dust particles and takes longer to reach the same filtration resistance.[42] The main reason for this is that conventional electrospinning nanofiber membranes are two-dimensional structures with limited space

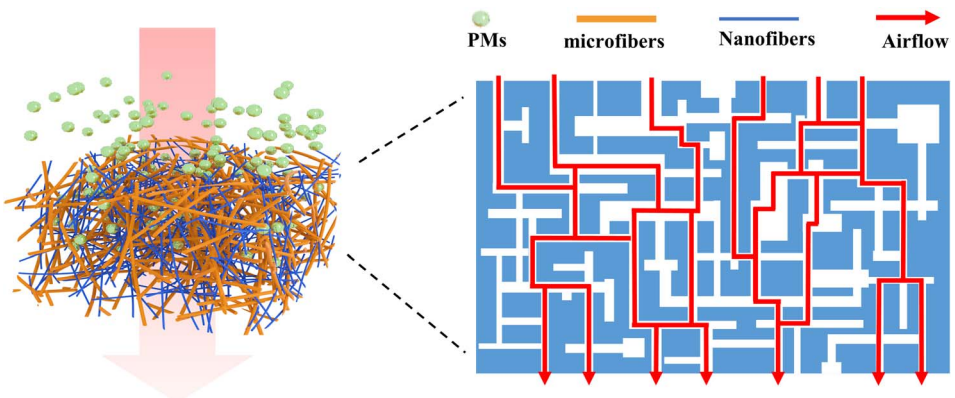

Fig. 7 A schematic explaining the filtration process of CBM for PMs.

to trap respirable particles. When conjugate electrospinning membranes are produced using double needles, they form a three-dimensional fluffy structure that provides more channels to facilitate the passage of air, leading to a decrease in pressure. Nanofibers are used to create a three-dimensional, porous structure that improves air circulation. This structure also increases the dust-holding capacity and reduces resistance by trapping PM in a larger area.[43–45] The use of micron fibers increases the size of the apertures and the center of the cavities, thereby improving the smooth airflow.

4. Conclusions

In conclusion, this study proposes the use of the conjugated electrostatic spinning technique to produce environmentally friendly PLA filters. The bimodal diameter distribution of the filter materials, combined with their enhanced filtering capacity and durability, makes them highly promising for the advancement of air filtration systems in the future. The method also emphasizes the use of a solvent mixture that is relatively environmentally friendly, aligning with the principles of green chemistry. The membrane fibers are distributed in a bimodal diameter distribution, which not only enhances the cavity structure of the filter but also effectively prevents the air channels from shrinking due to the fineness of the fibers. This fluffy structure enhances the physical interception of particulate matter by increasing the length of the pores. It has a high particle capacity, achieving a filtration efficiency of 99.94% for PM 0.3 and 99.96% for PM 2.5 at an airflow rate of 85 L min^{-1}. Its quality factor is also high, measuring 0.078 Pa^{-1} for PM 0.3 and 0.084 Pa^{-1} for PM 2.5. Furthermore, it demonstrates long-term stability with only a 2.35% decrease for PM 0.3 and a 0.05% decrease for PM 2.5 over a period of 60 days. Its dust holding capacity is excellent at 9.17 g m^{-2}. In comparison to the non-conjugated bimodal membrane, the conjugated membrane exhibits a 22.64% decrease in resistance. This work is significant in developing efficient, sustainable, and environmentally friendly solutions for air pollution control. It contributes to the knowledge and advancement of technologies for controlling air pollution.

Conflicts of interest

There are no conflicts to declare.

Acknowledgements

This research was funded by the Fujian Provincial Co-innovation Platform Project Program (No. 2021FX08). The authors are grateful to the Apparel of QNU for providing laboratory facilities.

Notes and references

1 X. X. Gong, C. Jin, X.-Y. Liu, J. Yu, S. Zhang and B. Ding, *Nano Lett.*, 2023, **23**, 1044–1051.
2 T. Dong, Y. Hua, G. Han, Y. Zhang, S. Chi, Y. Liu, C. Liu, C.-W. Lou and J.-H. Lin, *ACS Appl. Mater. Interfaces*, 2022, **14**, 37192–37203.
3 Y. Zhu, X. Gu, Z. Dong, B. Wang, X. Jin, Y. Chen, M. Cui, R. Wang and X. Zhang, *RSC Adv.*, 2023, **13**, 7857–7866.
4 E. Badillo-Goicoechea, T.-H. Chang, E. Kim, S. LaRocca, K. Morris, X. Deng, S. Chiu, A. Bradford, A. Garcia, C. Kern, C. Cobb, F. Kreuter and E. A. Stuart, *BMC Public Health*, 2021, **21**(1), 2099.
5 Y. Yang, Y. Yang, J. Huang, S. Li, Z. Meng, W. Cai and Y. Lai, *Adv. Fiber Mater.*, 2023, **5**, 1505–1518.
6 T. Lu, J. Cui, Q. Qu, Y. Wang, J. Zhang, R. Xiong, W. Ma and C. Huang, *ACS Appl. Mater. Interfaces*, 2021, **13**, 23293–23313.
7 W. Ma, W. Cao, T. Lu, R. Xiong and C. Huang, *J. Environ. Chem. Eng.*, 2022, **10**, 108908.
8 W. Cao, W. Ma, T. Lu, Z. Jiang, R. Xiong and C. Huang, *J. Colloid Interface Sci.*, 2022, **608**, 164–174.
9 K. Jin, S. Eyer, W. Dean, D. Kitto, F. S. Bates and C. J. Ellison, *Ind. Eng. Chem. Res.*, 2019, **59**, 5238–5246.
10 M. Jafari, E. Shim and A. Joijode, *Sep. Purif. Technol.*, 2021, **260**, 118185.
11 H. Gao, G. Liu, J. Guan, X. Wang, J. Yu and B. Ding, *Chem. Eng. J.*, 2023, **458**, 141412.
12 M. Gungor, S. Selcuk, A. Toptas and A. Kilic, *ACS Omega*, 2022, **7**, 46602–46612.
13 R.-R. Cai, S.-Z. Li, L.-Z. Zhang and Y. Lei, *Sci. Total Environ.*, 2020, **725**, 138297.
14 X. Cheng, Z. Zhang, L. Zhao, C. Deng, C. Li, Y. Du and M. Zhu, *J. Environ. Chem. Eng.*, 2023, **11**, 110561.
15 X. Li, G. Zhu, M. Tang, T. Li, C. Wang, X. Song, S. Zhang, J. Zhu, X. He, M. Hakkarainen and H. Xu, *ACS Appl. Mater. Interfaces*, 2023, **15**, 26812–26823.
16 T. T. Le, E. J. Curry, T. Vinikoor, R. Das, Y. Liu, D. Sheets, K. T. Tran, C. J. Hawxhurst, J. F. Stevens, J. N. Hancock, O. R. Bilal, L. M. Shor and T. D. Nguyen, *Adv. Funct. Mater.*, 2022, **32**(20), 2113040.
17 Y. Zhang, W. Ma, M. Lin, H. Qi and C. Zhang, *J. Text. Inst.*, 2023, 1–9.
18 L. Wang, Y. Gao, J. Xiong, W. Shao, C. Cui, N. Sun, Y. Zhang, S. Chang, P. Han, F. Liu and J. He, *J. Colloid Interface Sci.*, 2022, **606**, 961–970.
19 D. Gao, R. Zhao, X. Yang, F. Chen and X. Ning, *Membranes*, 2021, **11**, 819.
20 N. Wang, Y. Yang, S. S. Al-Deyab, M. El-Newehy, J. Yu and B. Ding, *J. Mater. Chem. A*, 2015, **3**, 23946–23954.
21 Y. Yang, S. Zhang, X. Zhao, J. Yu and B. Ding, *Sep. Purif. Technol.*, 2015, **152**, 14–22.
22 Y. Zhang, H. Xiao, R. Xiong and C. Huang, *Sep. Purif. Technol.*, 2023, **324**, 124513.
23 W. Ma, Z. Jiang, T. Lu, R. Xiong and C. Huang, *Chem. Eng. J.*, 2022, **430**, 132989.
24 W. Ma, W. Cao, T. Lu, R. Xiong and C. Huang, *J. Environ. Chem. Eng.*, 2022, **10**, 108908.
25 W. Cao, M. Zhang, W. Ma and C. Huang, *Sep. Purif. Technol.*, 2023, **327**, 124952.
26 Y. Zhang, X. Cui, X. Wang, X. Feng, Y. Deng, W. Cheng, R. Xiong and C. Huang, *Chem. Eng. J.*, 2023, **474**, 145804.

27 H. Liu, S. Zhang, L. Liu, J. Yu and B. Ding, *Adv. Funct. Mater.*, 2019, **29**, 1904108.
28 M. Tang, L. Jiang, C. Wang, X. Li, X. He, Y. Li, C. Liu, Y. Wang, J. Gao and H. Xu, *ACS Appl. Mater. Interfaces*, 2023, **15**, 25919–25931.
29 Z. Wang and Z. Pan, *Appl. Surf. Sci.*, 2015, **356**, 1168–1179.
30 X. Xie, D. Li, Y. Chen, Y. Shen, F. Yu, W. Wang, Z. Yuan, Y. Morsi, J. Wu and X. Mo, *Adv. Healthcare Mater.*, 2021, **10**(20), 2100918.
31 W. Han, D. Rao, H. Gao, X. Yang, H. Fan, C. Li, L. Dong and H. Meng, *Nano Energy*, 2022, **97**, 107237.
32 Y.-R. Chen, H.-W. Chung and S.-H. Tung, *ACS Appl. Polym. Mater.*, 2021, **3**, 5096–5104.
33 L. Kang, C. Ma, J. Wang, X. Gao and G. An, *Fibers Polym.*, 2023, **24**, 1975–1982.
34 X. Zhu, Z. Fan, X.-F. Zhang and J. Yao, *J. Colloid Interface Sci.*, 2023, **629**, 182–188.
35 J. Cui, T. Lu, F. Li, Y. Wang, J. Lei, W. Ma, Y. Zou and C. Huang, *J. Colloid Interface Sci.*, 2021, **582**, 506–514.
36 J. Liu, X. Zhang, H. Zhang, L. Zheng, C. Huang, H. Wu, R. Wang and X. Jin, *RSC Adv.*, 2017, **7**, 43879–43887.
37 X. Zhang, Y. Xu and Y. Zeng, *Fibers Polym.*, 2023, **24**, 1613–1621.
38 M. Kashif, H. Guo, J. Ge, X. Lv, S. Rasul and Y. Liu, *ACS Appl. Polym. Mater.*, 2023, **5**, 5995–6002.
39 M. E. Rosti, S. Pramanik, L. Brandt and D. Mitra, *Soft Matter*, 2020, **16**, 939–944.
40 W. Ma, H. Qi, Y. Zhang, M. Lin, Y. Qiu and C. Zhang, *Polymers*, 2023, **15**, 1459.
41 R. Xu, J. Feng, J. Qian, L. Zhang, S. Li, Y. Yang and X. Xi, *J. Membr. Sci.*, 2023, **685**, 121907.
42 Z. Han, L. Wang, Y. Liu, T. Chan, Z. Shi and M. Yu, *Sep. Purif. Technol.*, 2023, **314**, 123574.
43 G. Zheng, Z. Shao, J. Chen, J. Jiang, P. Zhu, X. Wang, W. Li and Y. Liu, *Nanomaterials*, 2021, **11**, 2567.
44 Z. Yang, X. Zhang, Z. Qin, H. Li, J. Wang, G. Zeng, C. Liu, J. Long, Y. Zhao, Y. Li and G. Yan, *Small*, 2022, **18**, 2107250.
45 Y. Deng, T. Lu, X. Zhang, Z. Zeng, R. Tao, Q. Qu, Y. Zhang, M. Zhu, R. Xiong and C. Huang, *J. Membr. Sci.*, 2022, **660**, 120857.